# Spectroscopic and HLCT Analysis on 4,7-Di(2-Thienyl)-2,1,3-Benzothiadiazole and Its Di-Substituted Derivatives for Development of Potent Hole Transport Material: DFT Approach

B. Felcia Merlin and R. Amrutha*

*Department of Physics, KCG College of Technology, Chennai-600097, India*

Received: 13.08.2021 & Accepted: 28.02.2022

Doi: 10.12693/APhysPolA.141.445 *e-mail: amrutha@kcgcollege.com

In the present study, the doping effect of the di-substitution of F, Cl, $CH_3$, $OCH_3$, OH, $NO_2$ to the reference donor–acceptor molecule 4,7-di-(2-thienyl)-2,1,3-benzothiadiazole (DTBT) has been reported by quantum chemical calculations in hybrid local charge transfer ($S_0 \rightarrow S_1$) state exciton process. The variation in molecular geometry confirms the charge transfer from the reference donor–acceptor unit to the substituted groups, except for the $CH_3$ substitution. The UV-Visible absorption, fluorescence emission, and Raman spectral characterization of the investigated systems validate the incidence of charge transfer. In frontier molecular orbital analysis, the decrease in the energy gap value of DTBT molecule after the addition of substituents indicates the intramolecular charge transfer from the donor–acceptor unit to the substituents, except for DTBT:$CH_3$. It also reveals higher charge carrier mobility in the investigated systems. The ionization potential, electron affinity, and re-organization energy analyses confirm that DTBT:OH molecular system causes the energy barriers to be reduced, displaying higher hole and electron transportability compared with the parent DTBT molecule and other substituents. The natural bond orbital analysis provides evidence that the DTBT:$OCH_3$, DTBT:OH, and DTBT:$NO_2$ molecular systems can be useful in the design of nonlinear optical materials. The natural population analysis confirms that the electron charge carrier mobility from the donor–acceptor unit to the substituted group increases upon the doping of halogen atoms. The calculated first-order hyperpolarizability value reveals that DTBT:$NO_2$ molecule has a higher value compared to that of all other investigated systems. Hence, the present study will be useful in the design of novel hole transport materials.

topics: 4,7-di-(2-thienyl)-2,1,3-benzothiadiazole, Raman, NLO, hole transport materials

## 1. Introduction

Thiophene- and benzothiadiazole-based donor–acceptor (D–A) conjugated materials have remarkable applications in the field of organic light-emitting diodes (OLEDs), dye-sensitized solar cells, and organic thin-film transistors [1, 2]. Thiophene-based organic semiconductors have unique characteristics due to their excellent hole-transport property [3]. In general, the hole transport and electron-accepting properties of D–A molecules can be useful for recognizing highly efficient OLED materials [4, 5]. Extensive research reported that $\pi$-conjugated organic material has a greater nonlinear optical (NLO) response than inorganic materials because of the D–A moieties, and they are used in the optical telecommunication, signal processing, and image transmission. Moreover, macroscopic $\pi$-conjugated materials with additional electron-withdrawing and donating groups on opposite sides enhance high charge carrier mobility and reduce the HOMO–LUMO gap, and these are the essential requirements for the rational design of OLED and NLO devices [6, 7].

The stable photo- and electroactive dithienylbenzothiazole are extensively studied for their high performance in electron/hole injection and transport properties [8]. J.C. Mei et al. [9] reported that the 4,7-di-2-thienyl-2,1,3-benzothiadiazole (DTBT) molecule has excellent hole transport and electron-accepting properties and also exhibits red light emission, which confirms that DTBT can be candidate in the design of OLED devices. Hung et al. [10] synthesized red light-emitting thiophene-based materials such as 4,7-bis(4-(4-s-butoxyphenyl)-5-(3,5-di(naphthalene-2-yl)phenyl)-thiopheneyl)benzo[c][1,2,5] thiadiazole, and reported their good hole-injection and

electron-transport properties in solid-state [10]. The poly [N-9'-heptadecanyl-2,7-carbazole-alt-5,5-(4,7-2-thinenyl-2,1,3-benzothiadiazole) is a low-bandgap and thermally stable thiophene-based copolymer widely used in the production of bulk-heterojunction photovoltaic devices [11].

Ohshita et al. [12] synthesized a thiophene-based polymer poly(dithienosilole-2,6-diyl) (DTD) and reported that DTD has good electrical conductivity and low charge carrier mobility, which proves that DTD can be useful in the design of hole transport materials. Recent studies reported that 4,7-di(5-bromo-2-thienyl)-2,1,3-benzothiadiazole (DTBT:Br) is used as a commercial organic molecular semiconductor. It is vital that the scientific community establish modifications to fine-tune the photoluminescent and electroluminescent behavior of this and other such semiconductors [13]. Some D–A molecules like 4-(anthracen-9yl)-N,N-dihenlaniline, 4-(phenanthren-9yl)-N,N-dihenlaniline and 4-(acridine-9yl)-N,N-dihenlaniline were designed and analyzed in HLCT excited state for the next-generation OLED materials [14]. Recently, the theoretical studies on the substitution effect of F, Cl, $CH_3$, $OCH_3$, OH, and $NO_2$ at the various position of benzo[2,3-b]thiopene have proved that it is an efficient hole transport material [15]. By keeping these parameters in mind, this work presents an unexplored Cl, $CH_3$, $OCH_3$, OH, and $NO_2$ substitution in a potential OLED molecule 4,7-di-(2-thienyl)-2,1,3-benzothiadiazole (DTBT). These have been extensively studied in HLCT state, using density functional theory (DFT) and time-dependent density functional theory (TD-DFT) to demonstrate the excellent performance of hole transport materials for OLED and NLO application.

## 2. Materials and methods

### 2.1. Materials

In this study,

- 4,7-di-(2-thienyl)-2,1,3-benzothiadiazole (DTBT),
- 4,7-di(5-fluro-2-thienyl)-2,1,3-benzothiadiazole (DTBT:F),
- 4,7-di(5-chloro-2-thienyl)-2,1,3-benzothiadiazole (DTBT:Cl),
- 4,7-di(5-methyl-2-thienyl)-2,1,3-benzothiadiazole (DTBT:$CH_3$),
- 4,7-di(5-methoxy-2-thienyl)-2,1,3-benzothiadiazole (DTBT:$OCH_3$),
- 4,7-di(5-hydroxy-2-thienyl)-2,1,3-benzothiadiazole (DTBT:OH),
- 4,7-di(5-nitro-2-thienyl)-2,1,3-benzothiadiazole (DTBT:$NO_2$)

have been designed and used.

### 2.2. Computational details

The molecular structures of the DTBT, DTBT:F, DTBT:Cl, DTBT:$CH_3$, DTBT:$OCH_3$, DTBT:OH, and DTBT:$NO_2$ molecular systems were optimized by the DFT/B3LYP method with a 6-311+G$(d,p)$ basis set using the commercially available Gaussian 09 [16] program. Raman spectra of the investigated molecular systems were simulated using DFT/B3LYP method with a 6-311+G$(d,p)$ basis set. The UV-Visible (UV-Vis) absorption and emission spectra of the investigated molecular systems were simulated using the TD-DFT/B3LYP and TD-CAM-B3LYP functional with a 6-311+G$(d,p)$ basis set. The optimized molecular structure, vibrational spectra and frontier molecular orbitals (FMO) of the molecular systems were visualized using GaussView 5.0 [17].

The calculated vibrational frequencies were assigned without imposing any symmetry constraints by employing the same functional and basis set using VEDA 4.0 program [18]. The optimized molecular structure was used to find the properties such as ionization potential, electron affinity, and reorganization energy. The natural bond orbital analysis and natural population analysis were performed to identify the charge transfer between the D–A unit and substituted groups of the DTBT molecule. The first-order hyperpolarizability values of the investigated molecular systems were calculated using the DFT/B3LYP method with 6-311+G$(d,p)$ basis set.

## 3. Results and discussion

### 3.1. Molecular geometry and charge transfer analysis

The optimized molecular geometry of the DTBT, DTBT:F, DTBT:Cl, DTBT:$CH_3$, DTBT:$OCH_3$, DTBT:OH, and DTBT:$NO_2$ molecular systems are depicted in Fig. 1. A few significant bond length values in their excited, ground, cationic, and anionic states are listed in Table I. The variation in the bridge bond length in optimized $S_1$ state geometry is $< S_0$ state geometry for both electron-withdrawing (F and Cl) and electron-donating groups ($CH_3$, $OCH_3$, and OH) of substituted DTBT molecules. Upon substitution, all the bridge bond lengths in the $S_1$ states are shortened, as mentioned in Table I. Note that, upon substitution, the bond length in the $S_1$ states exceeds the bond length in the $S_0$ states, except for $CH_3$ substitution, where the bond length is marginally shorter. This indicates the electron-withdrawing nature of the substituted atoms. On the other hand, there is a decrease in the substituted bond length in methoxy- and hydroxy-thienyl-benzothiadiazole in $S_1$ state to 1.32 Å and 1.34 Å, respectively, compared to the values of CO bond lengths stated by Demainson et al. [19] (1.38 Å to 1.42 Å). The mentioned decrease confirms the electron-donating nature of the oxygen

TABLE I

The most important bond length values in their excited, ground, cationic and anionic states of DTBT, DTBT:F, DTBT:Cl, DTBT:$CH_3$, DTBT:$OCH_3$, DTBT:OH, and DTBT:$NO_2$ molecular systems calculated using B3LYP/6-311+G$(d,p)$.

| Compound | Inter-ring bond length | Excited state $S_1$ [Å] | Ground state $S_0$ [Å] | Excited cationic state [Å] | Excited anionic state [Å] |
|---|---|---|---|---|---|
| 4,7-di-(2-thienyl)-2,1,3-benzothiadiazole | C13–H24 | 1.082 | 1.081 | 1.083 | 1.082 |
| (DTBT) | C6–C15 | 1.433 | 1.458 | 1.423 | 1.447 |
| 4,7-di(5-fluro-2-thienyl)-2,1,3-benzothiadiazole | C13–F15 | 1.432 | 1.332 | 1.311 | 1.349 |
| (DTBT:F) | C6–C16 | 1.326 | 1.456 | 1.421 | 1.446 |
| 4,7-di(5-chloro-2-thienyl)-2,1,3-benzothiadiazole | C13–Cl 15 | 1.430 | 1.331 | 1.704 | 1.746 |
| (DTBT:Cl) | C6–C16 | 1.427 | 1.450 | 1.423 | 1.444 |
| 4,7-di(5-methyl-2-thienyl)-2,1,3-benzothiadiazole | C18–C20 | 1.326 | 1.440 | 1.493 | 1.497 |
| (DTBT:$CH_3$) | C6–C15 | 1.432 | 1.456 | 1.445 | 1.445 |
| 4,7-di(5-methoxy-2-thienyl)-2,1,3-benzothiadiazole | C20–O22 | 1.346 | 1.326 | 1.316 | 1.368 |
| (DTBT:$OCH_3$) | C6–C17 | 1.432 | 1.452 | 1.418 | 1.448 |
| 4,7-di(5-hydroxy-2-thienyl)-2,1,3-benzothiadiazole | C13–O15 | 1.370 | 1.345 | 1.326 | 1.374 |
| (DTBT:OH) | C9–C10 | 1.370 | 1.446 | 1.418 | 1.446 |
| 4,7-di(5-nitro-2-thienyl)-2,1,3-benzothiadiazole | C13–N15 | 1.424 | 1.423 | 1.453 | 1.401 |
| (DTBT:$NO_2$) | N15–O17 | 1.270 | 1.269 | 1.224 | 1.248 |
| | N15–O16 | 1.270 | 1.270 | 1.229 | 1.250 |
| | C9–C10 | 1.424 | 1.424 | 1.426 | 1.433 |

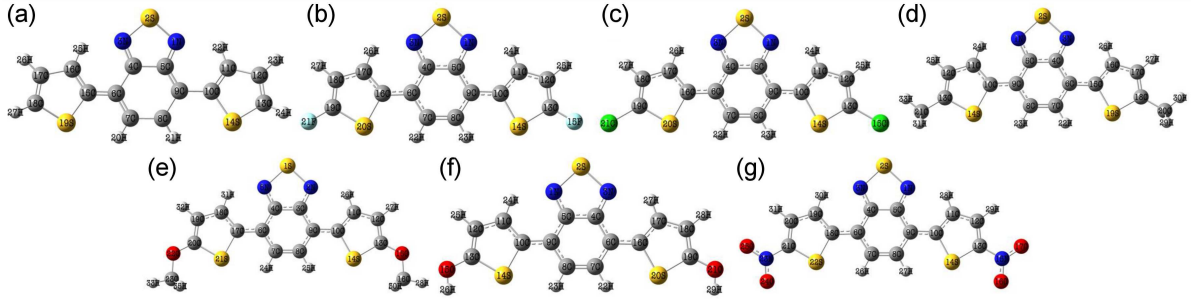


Fig. 1. The optimized molecular geometries of (a) DTBT, (b) DTBT:F, (c) DTBT:Cl, (d) DTBT:$CH_3$, (e) DTBT:$OCH_3$, (f) DTBT:OH and (g) DTBT:$NO_2$ molecular systems, computed using B3LYP/6-311+G$(d,p)$.

atoms to the D–A unit. We can infer that there is a significant charge transfer from the D–A unit to most of the substituted groups and it is attributed to significant electrostatic interaction between the D–A unit and substituted groups.

The bridge bond length value upon the substitution of the known electron-withdrawing $NO_2$ functional group was calculated as 1.424 Å for C9–C10 and C6–C18. The bond length values of the bond connecting the $NO_2$ substitutions and DTBT molecule were calculated as 1.424Å for C13–N15 and C21–N23. This equality in bond length values indicates that the hypervalent sulphur atom of thiophene creates an inductive electron-donating effect in the $NO_2$ groups and shows a balanced carrier transport of electrons of both $NO_2$ groups to the D–A unit with holes. The calculated cationic state bond length values of all DTBT derivatives are smaller then in the anionic state, resulting in more polarization of anions in the molecular system, which is due to the low hole-reorganization energy ($\lambda_h$) [15]. In Table II, the dihedral angle involving the bridge bond between thiophene and 2,1,3-benzothiadiazole, along with its substituted F, Cl, and $NO_2$ molecular systems, is about ±179.99°. The substitution of F, Cl, and $NO_2$ exhibits a planar structure. This planar geometry influences a strong coupling effect in the substituted groups so that the electrons can move more freely from the D–A unit to the substituted groups.

The dihedral angle for DTBT:OH is nearly 0°, indicating a strong push–pull effect between the D–A unit and OH group. The average of two dihedrals of DTBT:$OCH_3$ and DTBT:$CH_3$ is 61°. Hence

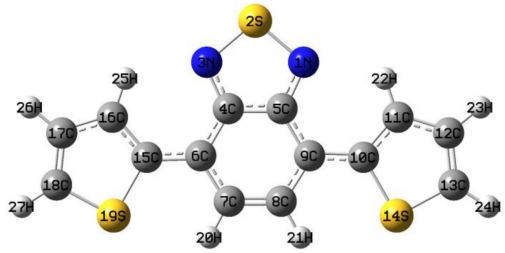


Fig. 2. The optimized molecular geometries of DTBT molecular system, computed using CAM-B3LYP/6-311+G$(d,p)$.

TABLE II

The most important Dihedral angle values in their ground, excited states of DTBT, DTBT:F, DTBT:Cl, DTBT:$CH_3$, DTBT:$OCH_3$, DTBT:OH, and DTBT:NO2 molecular systems calculated using B3LYP/6-311+G$(d,p)$.

| Compound | Dihedral angle | $S_0$ | $S_1$ |
|---|---|---|---|
| DTBT | C7–C6–C15–C16 | 179.61 | 179.97 |
| DTBT:F | C7–C6–C16–C17 | 179.98 | 179.99 |
| DTBT:Cl | C7–C6–C16–C17 | 179.98 | 179.99 |
| DTBT:$CH_3$ | S19–C18–C20–H28 | 60.28 | 60.03 |
| DTBT:$OCH_3$ | C20–O22–C23–H35 | 61.05 | 61.02 |
| DTBT:OH | S14-C13-O15-H26 | 0.01 | 0.00 |
| DTBT:$NO_2$ | C8–C9–C10–C11 | 179.99 | 180.00 |

twisting charge transfer occurs in DTBT:$OCH_3$ and DTBT:$CH_3$ with the mixing of HLCT state, suggesting higher electron transfer to the D–A unit from substituted groups [14–20]. The compared results of the DTBT molecular system, calculated using B3LYP/6-311+G$(d,p)$ with CAM-B3LYP/6-311+G$(d,p)$, are in similar agreement, as shown in Fig. 2 and Tables III and IV. The structural differences in all the rotamers specify that the potential energy barrier around rotation about C–C bonds that connect the central unit has lesser C–C bond lengths in the $S_1$ state than in the $S_0$ state. The shortening of central terminal C6–C16 and C9–C10 of, respectively, F and OH in the $S_1$ state corresponds to large rotational barriers that correlate with the strength of $\pi$-conjugation in the rotamers. This change indicates that the increases of potential energy in the ground state ($S_0$) causes a repulsive steric interaction in the excited state ($S_1$), followed by molecules with substituents Cl, $CH_3$, $OCH_3$, and $NO_2$ dramatically reducing the barrier for charge transfer in the lowest singlet electronic states ($S_0 \rightarrow S_1$).

### 3.2. Absorption and emission spectral analysis

The effect of substitution in the UV-Visible spectra and the corresponding electronic transitions of the molecule were predicted using the

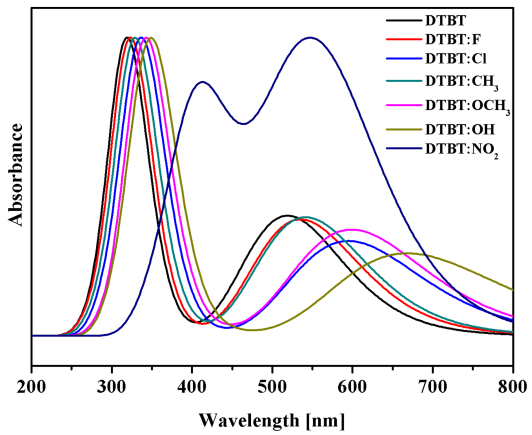


Fig. 3. The UV-Visible absorption spectra of the DTBT, DTBT:F, DTBT:Cl, DTBT:$CH_3$, DTBT:$OCH_3$, DTBT:OH, and DTBT:$NO_2$ molecular systems, simulated using TD-B3LYP/6-311+G$(d,p)$.

TABLE III

The most important bond length values in their excited ($S_1$), ground ($S_0$), cationic and anionic states of DTBT.

| Inter-ring bond length | $S_1$ [Å] | $S_0$ [Å] | Excited cationic state [Å] | Excited anionic state [Å] |
|---|---|---|---|---|
| C13–H24 | 1.081 | 1.080 | 1.083 | 1.080 |
| C6–C15 | 1.430 | 1.452 | 1.423 | 1.444 |

TABLE IV

The most important dihedral angle values in their ground ($S_0$), excited states ($S_1$) of DTBT by CAM-B3LYP/6-311+G$(d,p)$.

| Dihedral angle | $S_0$ | $S_1$ |
|---|---|---|
| C7–C6–C15–C16 | 180.51 | 179.95 |

TD-DFT/B3LYP method with 6-311+G$(d,p)$ basis set. The TD-DFT calculation is a powerful tool for investigating the static and dynamic properties of the molecules in their excited states [21]. The simulated UV-Visible absorption and emission spectra of the DTBT, DTBT:F, DTBT:Cl, DTBT:$CH_3$, DTBT:$OCH_3$, DTBT:OH, and DTBT:$NO_2$ molecular systems obtained using TD-B3LYP and TD-CAM-B3LYP are shown in Figs. 3–6, respectively. The calculated electronic transitions, absorption wavelength ($\lambda$), excitation energies ($E$), and oscillator strength ($f$) in the gas phase for all investigated systems are listed in Table V and VI. In addition, the calculated electronic transitions, emission wavelength ($\lambda$), excitation energies ($E$), and oscillator strength ($f$) in the gas phase for all investigated systems are listed in Tables VII and VIII.

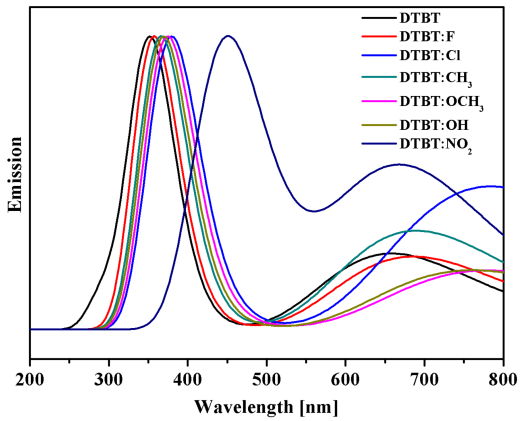


Fig. 4. The UV-Visible emission spectra of the DTBT, DTBT:F, DTBT:Cl, DTBT:$CH_3$, DTBT:$OCH_3$, DTBT:OH, and DTBT:$NO_2$ molecular systems, simulated using TD-B3LYP/6-311+G$(d,p)$.

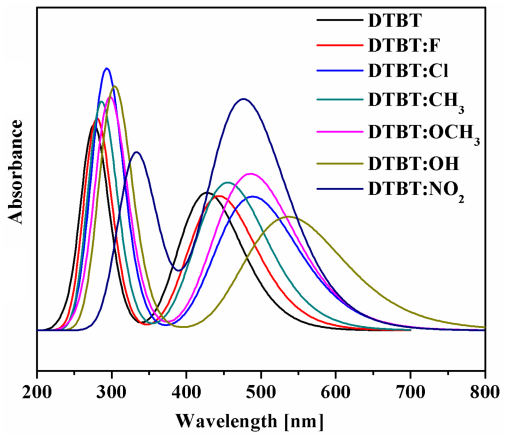


Fig. 5. The UV-Visible absorption spectra of the DTBT, simulated using TD-CAM-B3LYP/6-311+G$(d,p)$.

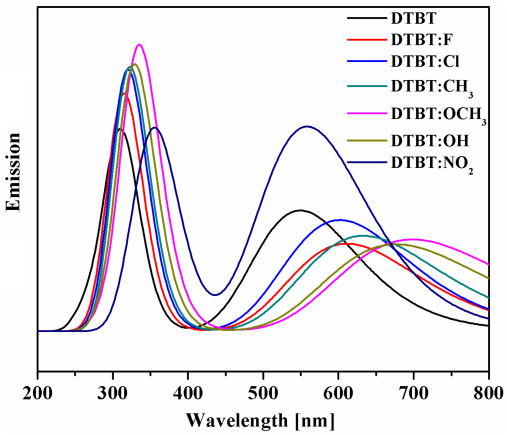


Fig. 6. The UV-Visible emission spectra of the DTBT, simulated using TD-CAM-B3LYP/6-311+G$(d,p)$.

TABLE V

The electronic transitions, absorption wavelength ($\lambda$), excitation energies ($E$) and oscillator strength ($f$) in gas phase for the DTBT, DTBT:F, DTBT:Cl, DTBT:$CH_3$, DTBT:$OCH_3$, DTBT:OH, and DTBT:$NO_2$ molecular systems, calculated using TD-B3LYP/6-311+G$(d,p)$.

| Compound | Electronic transitions | $\lambda$ [nm] | $E$ [eV] | $f$ | State |
|---|---|---|---|---|---|
| DTBT | $S_0 \to S_1$ | 525 | 2.387 | 0.278 | $\pi \to \pi^*$ |
| | $S_0 \to S_3$ | 335 | 4.228 | 0.097 | $n \to \pi^*$ |
| DTBT:F | $S_0 \to S_1$ | 555 | 2.316 | 0.274 | $\pi \to \pi^*$ |
| | $S_0 \to S_3$ | 349 | 4.229 | 0.084 | $n \to \pi^*$ |
| DTBT:Cl | $S_0 \to S_1$ | 598 | 2.084 | 0.271 | $\pi \to \pi^*$ |
| | $S_0 \to S_3$ | 351 | 3.966 | 0.000 | $n \to \pi^*$ |
| DTBT:$CH_3$ | $S_0 \to S_1$ | 551 | 2.288 | 0.315 | $\pi \to \pi^*$ |
| | $S_0 \to S_3$ | 338 | 4.204 | 0.097 | $n \to \pi^*$ |
| DTBT:$OCH_3$ | $S_0 \to S_1$ | 620 | 2.070 | 0.295 | $\pi \to \sigma^*$ |
| | $S_0 \to S_3$ | 316 | 4.147 | 0.057 | $n \to \sigma^*$ |
| DTBT:OH | $S_0 \to S_1$ | 668 | 1.855 | 0.225 | $\pi \to \sigma^*$ |
| | $S_0 \to S_3$ | 363 | 3.665 | 0.128 | $n \to \sigma^*$ |
| DTBT:$NO_2$ | $S_0 \to S_1$ | 555 | 2.246 | 0.566 | $\pi \to \pi^*$ |
| | $S_0 \to S_3$ | 407 | 3.358 | 0.001 | $n \to \pi^*$ |

TABLE VI

The electronic transitions, absorption wavelength ($\lambda$), excitation energies ($E$) and oscillator strength ($f$) in the gas phase for the DTBT molecular system, calculated using TD-CAM-B3LYP/6-311+G$(d,p)$.

| Compound | Electronic transitions | $\lambda$ [nm] | $E$ [eV] | $f$ | State |
|---|---|---|---|---|---|
| DTBT | $S_0 \to S_1$ | 427 | 2.897 | 0.421 | $\pi \to \pi^*$ |
| | $S_0 \to S_3$ | 260 | 5.429 | 0.000 | $n \to \pi^*$ |
| DTBT:F | $S_0 \to S_1$ | 470 | 3.114 | 0.574 | $\pi \to \pi^*$ |
| | $S_0 \to S_3$ | 270 | 6.542 | 0.073 | $n \to \pi^*$ |
| DTBT:Cl | $S_0 \to S_1$ | 510 | 3.154 | 0.642 | $\pi \to \pi^*$ |
| | $S_0 \to S_3$ | 310 | 6.628 | 0.175 | $n \to \pi^*$ |
| DTBT:$CH_3$ | $S_0 \to S_1$ | 470 | 4.288 | 0.725 | $\pi \to \pi^*$ |
| | $S_0 \to S_3$ | 280 | 7.246 | 0.224 | $n \to \pi^*$ |
| DTBT:$OCH_3$ | $S_0 \to S_1$ | 510 | 5.070 | 0.835 | $\pi \to \sigma^*$ |
| | $S_0 \to S_3$ | 330 | 7.579 | 0.348 | $n \to \sigma^*$ |
| DTBT:OH | $S_0 \to S_1$ | 560 | 4.456 | 0.950 | $\pi \to \sigma^*$ |
| | $S_0 \to S_3$ | 340 | 8.735 | 0.468 | $n \to \sigma^*$ |
| DTBT:$NO_2$ | $S_0 \to S_1$ | 490 | 3.276 | 0.543 | $\pi \to \pi^*$ |
| | $S_0 \to S_3$ | 350 | 5.328 | 0.019 | $n \to \pi^*$ |

As shown in Fig. 3, the first peak was at 335, 349, 351, 338, 316, 363 and 407 nm, corresponding to a ground population. The second peak was observed at 525, 555, 598, 551, 620, 668 and 555 nm. In Fig. 4 the situation changes. The excitation causes overlapping of emission bands and manifests the dual emission. The strong red-shift in the presented molecular species indicates the ability to separate the energy barrier in the excited state intramolecular charge transfer. We can compare the absorption and emission wavelength of DTBT obtained with TD-B3LYP (525 and 658 nm, respectively)

TABLE VII

The electronic transitions, emission wavelength ($\lambda$), emission energies ($E$) and oscillator strength ($f$) in gas phase for the DTBT, DTBT:F, DTBT:Cl, DTBT:$CH_3$, DTBT:$OCH_3$, DTBT:OH, and DTBT:$NO_2$ molecular systems, calculated using TD-B3LYP/6-311+G($d,p$).

| Compound | Electronic transitions | $\lambda$ [nm] | $E$ [eV] | $f$ | State |
|---|---|---|---|---|---|
| DTBT | $S_0 \leftarrow S_1$ | 658 | 1.882 | 0.192 | $\pi \rightarrow \pi^*$ |
| | $S_0 \leftarrow S_3$ | 359 | 4.074 | 0.076 | $n \rightarrow \pi^*$ |
| DTBT:F | $S_0 \leftarrow S_1$ | 684 | 1.808 | 0.183 | $\pi \rightarrow \pi^*$ |
| | $S_0 \leftarrow S_3$ | 362 | 3.044 | 0.006 | $n \rightarrow \pi^*$ |
| DTBT:Cl | $S_0 \leftarrow S_1$ | 783 | 1.582 | 0.170 | $\pi \rightarrow \pi^*$ |
| | $S_0 \leftarrow S_3$ | 443 | 2.795 | 0.006 | $n \rightarrow \pi^*$ |
| DTBT:$CH_3$ | $S_0 \leftarrow S_1$ | 689 | 1.797 | 0.214 | $\pi \rightarrow \pi^*$ |
| | $S_0 \leftarrow S_3$ | 365 | 3.014 | 0.008 | $n \rightarrow \pi^*$ |
| DTBT:$OCH_3$ | $S_0 \leftarrow S_1$ | 780 | 1.588 | 0.186 | $\pi \rightarrow \pi^*$ |
| | $S_0 \leftarrow S_3$ | 374 | 2.752 | 0.013 | $n \rightarrow \pi^*$ |
| DTBT:OH | $S_0 \leftarrow S_1$ | 760 | 1.617 | 0.174 | $\pi \rightarrow \pi^*$ |
| | $S_0 \leftarrow S_3$ | 369 | 2.803 | 0.009 | $n \rightarrow \pi^*$ |
| DTBT:$NO_2$ | $S_0 \leftarrow S_1$ | 671 | 1.845 | 0.383 | $\pi \rightarrow \pi^*$ |
| | $S_0 \leftarrow S_3$ | 470 | 2.750 | 0.689 | $n \rightarrow \pi^*$ |

TABLE VIII

The electronic transitions, emission wavelength ($\lambda$), emission energies ($E$) and oscillator strength ($f$) in the gas phase for the DTBT molecular system, calculated using TD-CAM-B3LYP/6-311+G($d,p$).

| Compound | Electronic transitions | $\lambda$ [nm] | $E$ [eV] | $f$ | State |
|---|---|---|---|---|---|
| DTBT | $S_0 \leftarrow S_1$ | 549 | 2.257 | 0.367 | $\pi \rightarrow \pi^*$ |
| | $S_0 \leftarrow S_3$ | 290 | 5.100 | 0.000 | $n \rightarrow \pi^*$ |
| DTBT:F | $S_0 \leftarrow S_1$ | 620 | 1.200 | 0.161 | $\pi \rightarrow \pi^*$ |
| | $S_0 \leftarrow S_3$ | 310 | 3.002 | 0.001 | $n \rightarrow \pi^*$ |
| DTBT:Cl | $S_0 \leftarrow S_1$ | 590 | 1.542 | 0.120 | $\pi \rightarrow \pi^*$ |
| | $S_0 \leftarrow S_3$ | 340 | 2.424 | 0.012 | $n \rightarrow \pi^*$ |
| DTBT:$CH_3$ | $S_0 \leftarrow S_1$ | 630 | 1.624 | 0.124 | $\pi \rightarrow \pi^*$ |
| | $S_0 \leftarrow S_3$ | 340 | 3.010 | 0.001 | $n \rightarrow \pi^*$ |
| DTBT:$OCH_3$ | $S_0 \leftarrow S_1$ | 680 | 1.541 | 0.142 | $\pi \rightarrow \pi^*$ |
| | $S_0 \leftarrow S_3$ | 340 | 2.251 | 0.011 | $n \rightarrow \pi^*$ |
| DTBT:OH | $S_0 \leftarrow S_1$ | 670 | 1.102 | 0.151 | $\pi \rightarrow \pi^*$ |
| | $S_0 \leftarrow S_3$ | 350 | 2.001 | 0.004 | $n \rightarrow \pi^*$ |
| DTBT:$NO_2$ | $S_0 \leftarrow S_1$ | 570 | 1.428 | 0.323 | $\pi \rightarrow \pi^*$ |
| | $S_0 \leftarrow S_3$ | 360 | 2.263 | 0.458 | $n \rightarrow \pi^*$ |

shown in Fig. 3, 4 and Tables V, VII, with those obtained with TD-CAM-B3LYP (427 and 549 nm, respectively) shown in Figs. 5 and 6 and Tables VI and VIII. The appearance of the blue shift in the absorptions spectra 427 nm of DTBT with through TD-CAM-B3LYP is attributed to charge transfer between the D–A unit. The appearance of redshift 658 nm in the emission spectra of DTBT obtained using TD-B3LYP indicates that the emission takes place with a longer wavelength. It is evident from TD-B3LYP functional (see Fig. 4) that the maximum emission peaks are longer for wavelengths, ranging from $\geq$ 671 nm for $NO_2$ and from $\leq$ 783 nm for Cl substitution predicted. These results show that the emission spectra are located in the far visible region. Comparing the substitution with TD-CAM-B3LYP wavelength ranges (see Fig. 6), i.e., from $\geq$ 570 nm for $NO_2$ substitution predicted and $\leq$ 680 nm for $OCH_3$ substitution predicted, it turns out that their emission spectra are located in the red visible region. Hence TD-CAM-B3LYP acts as an efficient tool in the emission spectral calculation.

Rotamers in ground state $S_0$ commonly have a very small population due to high energy barriers. The dynamics of excited state intramolecular effect on alkyl substitutions of $CH_3$, $OCH_3$, and OH to the rotamer of 2,5-bis-2-benzoxazolyl-phenol displays dual emission with redshift [22]. The effect of chemical substitution of $CH_3$ onto the molecular frame of 7-hydroxyquinoline on the energetical landscape of ground and the lowest singlet excited state ($S_0 \rightarrow S_1$) is the increase in $\pi$ orbital interaction, which was shown to occur in $S_0$ with $n \rightarrow \pi^*$ transition and in $S_1$ with $\pi \rightarrow \pi^*$ transition [23]. The effect of the chemical substitutions of $NO_2$ on the molecular structure of 3-hydroxy-picolinic acid ($S_0 \leftarrow S_1$) was identified with $S_0$ ($n \rightarrow \pi^*$) $S_1$ ($\pi \rightarrow \pi^*$) [24].

The electronic spectra of thiazolo-[3,2-a]pyridine with electron donating groups $CH_3$ and $OCH_3$ carried out by TD-CAM-B3LYP manifest that the substituent effect on the core molecule undergoes $n \rightarrow \sigma^*$ transition at 373 nm and $\pi \rightarrow \sigma^*$ transition at longer wavelengths [25]. The optical excitation with chemical modification on DTBT and its derivatives upon the reactive state ($S_0 \rightarrow S_1$) increases the energy barrier values in the vicinity of $n \rightarrow \pi^*$ transition and electronically excited state ($S_0 \rightarrow S_3$) decreases the energy barrier values in the vicinity of $\pi \rightarrow \pi^*$ electronic transition responsible for the potential OLED application. Among all the systems studied, it was observed in Fig. 3 and Table V, obtained using TD-B3LYP, that the absorption spectra of DTBT:OH with a maximum wavelength 668 nm are manifested (Bathochromic shift of the absorption spectrum) and a lower bandgap 2.20 eV requires higher charge carrier mobility. By comparing the absorption spectra, using TD-CAM-B3LYP it was again observed that DTBT:OH has a maximum wavelength of 560 nm, as shown in Fig. 5 and Table VI. It follows that the OH substituent exhibits a strong $\pi$-electron-donating and $\sigma^*$-electron-accepting character, resulting in longer absorption wavelength.

The study of dipole moment in electronically first excited singlet-state is significant as it provides useful information for designing novel NLO materials. In general, the energy transfer from the excited state of the substituted D–A unit to the ground state leads to a long-range dipole–dipole interaction [26]. In the present case, the DTBT:$NO_2$ system exhibits a larger dipole moment

TABLE IX

The calculated vibrational wave numbers and assignments of the DTBT, DTBT:F, DTBT:Cl, DTBT:$CH_3$, DTBT:$OCH_3$, DTBT:OH, and DTBT:$NO_2$ molecular systems. The symbol $\nu$ denotes stretching, $\nu_s$ — symmetric stretching, $\beta$ — in-plane bending, $\delta$ — scissoring, $\rho$ — rocking, $\zeta$ — deformations, $\Theta$ — thiophene ring, and $\varphi$ — benzothiadiazole ring. PED represents potential energy distribution.

| Calculated wavenumbers [$cm^{-1}$] | | | | | | | Assignment |
|---|---|---|---|---|---|---|---|
| DTBT | DTBT:F | DTBT:Cl | DTBT:$CH_3$ | DTBT:$OCH_3$ | DTBT:OH | DTBT:$NO_2$ | (PED [%]) |
| 1584 | 1585 | 1583 | 1584 | 1585 | 1585 | 1579 | $\nu\varphi$ C–C (29), $\beta\varphi$ C–H (10) |
| 1534 | 1532 | 1534 | 1530 | 1541 | 1536 | 1537 | $\nu\varphi$ C–N (17), $\rho\varphi$ C–H (11), $\nu\Theta$ C=C (13), $\zeta$ C–$H_3$ (16), $\nu$ C–O (10), $\beta$ O–H (12) |
| – | – | – | 1512 | – | – | – | $\nu\Theta$ C=C (13), $\zeta$ C–$H_3$ (14) |
| 1487 | – | 1490 | – | 1483 | – | 1480 | $\nu\Theta$ C–C (13), $\nu\Theta$ C=C (10), $\beta\Theta$ C–H (10) |
| 1422 | 1416 | 1413 | 1414 | 1420 | 1430 | 1420 | $\nu\Theta$ C–C (17), $\nu\Theta$ C=C (17) |
| – | – | – | – | – | – | 1494 | $\nu\Theta$ C–C (13), $\nu\varphi$ C–C (22), $\nu$ C–N (38) |
| 1384 | 1377 | 1373 | 1375 | 1381 | 1387 | 1377 | $\nu\Theta$ C–C (16), $\nu\Theta$ C=C (18), $\nu\varphi$ C-N (11), $\nu_s NO_2$ (31) |
| 1347 | 1347 | 1346 | 1346 | 1346 | 1348 | 1348 | $\nu\varphi$ C–N (28), $\delta\varphi$ C–H (11) |
| – | 1269 | – | 1267 | 1292 | 1276 | 1260 | $\beta\varphi$C–H (52) |
| 1146 | 1147 | 1147 | 1146 | 1146 | 1146 | 1148 | $\delta\varphi$ C–H (11), $\beta\Theta$ C–H (23) |
| 1083 | 1065 | 1099 | 1086 | 1077 | 1067 | 1065 | $\delta\Theta$ C–H (43) |

value of 5.1651 D (5.1651 Debye) compared to that of all the other investigated systems, which leads to a high degree of first-order hyperpolarizability of the DTBT:$NO_2$ system.

### 3.3. Raman spectral analysis

Raman spectral analysis using DFT calculations is potentially important as a low-cost tool for the functional group analysis of drugs, bioactive molecules, and NLO materials [27]. In order to investigate the intramolecular interaction between DTBT and its substitutions a DFT simulated Raman spectra of DTBT, DTBT:F, DTBT:Cl, DTBT:$CH_3$, DTBT:$OCH_3$, DTBT:OH, and DTBT:$NO_2$ molecular systems obtained using B3LYP/6-311+G$(d,p)$ are shown in Fig. 7. The Raman spectra of the DTBT molecular system obtained using CAM-B3LYP/6-311+G$(d,p)$ (see Fig. 8) show a similar agreement as the DTBT obtained using B3LYP. The calculated vibrational wavenumbers and their corresponding assignments are listed in Table IX. In the DTBT molecule, a strong peak was calculated at 1564 $cm^{-1}$, which is due to the C–C and C=C stretching of bithiophene [28]. Significantly, a very weak vibrational mode was calculated at 1480 $cm^{-1}$ in the DTBT molecule. This vibrational mode arises from the broad C–C and C=C stretching of bithiophenes and benzothiadiazole [29].

The substitution peak position of DTBT:F was observed to be at 1585, 1591, 1620, 1648, 1676, and 1597 $cm^{-1}$ for the DTBT:F, DTBT:Cl, DTBT:$CH_3$, DTBT:$OCH_3$, DTBT:OH, and DTBT:$NO_2$ molecular systems, respectively. The peak identified at 1585, 1591, and 1597 $cm^{-1}$ for F, Cl, and $NO_2$, respectively, can be attributed

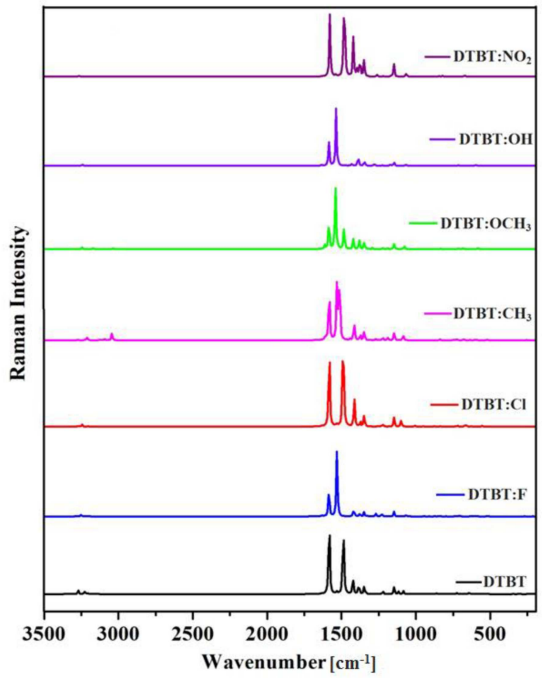


Fig. 7. The Raman spectra of (a) DTBT, (b)DTBT:F, (c) DTBT:Cl, (d)DTBT:$CH_3$, (e) DTBT:$OCH_3$, (f) DTBT:OH and (g) DTBT:$NO_2$ molecular systems, simulated using B3LYP/6-311+G$(d,p)$.

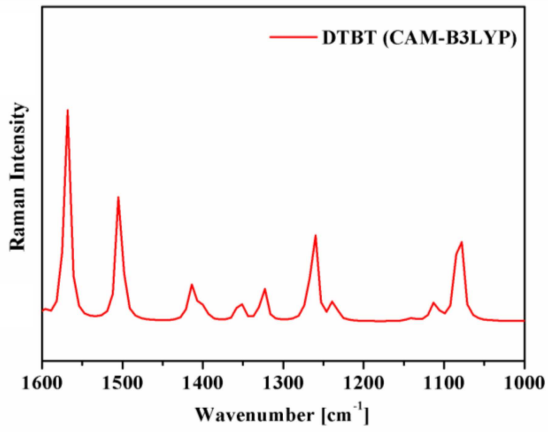


Fig. 8. The Raman spectra of DTBT molecular systems, simulated using CAM-B3LYP/6-311+G$(d,p)$.

to the coupled vibrations of the C–H symmetric wagging of the benzothiadiazole ring and C–H asymmetric wagging of thiophene rings. In the case of benzothiadiazole and the electron-withdrawing $NO_2$, the symmetric stretching appears. Hence the completely symmetric vibrational modes indicating redshift with the heteroaromatic structure, where the charge transfer takes place from the D–A unit to the substituents (intramolecular CT), resulting in softening of the bithienyl molecule. The peak was identified at 1620, 1648, and 1676 $cm^{-1}$ for $CH_3$, $OCH_3$, and OH substitution, respectively. The symmetric $CH_3$ stretching confirms the intermolecular CT correlated with FMO. The (C=O) stretching of the $OCH_3$ group provides a partial heteroaromatic/heteroquinoniod structure (partial inter/intramolecular CT) character. Raman analysis of O–H stretching in a single water molecule gives the result of 3150 $cm^{-1}$.

It is carefully studied, as C–O stretching and O–H bending modes are dependent vibrational modes [30], and they are coupled with the adjacent C–C and C=C stretching of the D–A unit, confirming higher intermolecular and higher intramolecular CT character [31]. Moreover, small peaks are calculated at 1422, 1416, 1413, 1414, 1420, 1430 and 1420 $cm^{-1}$ and 1384, 1377, 1373, 1375, 1381, 1387 and 1377 $cm^{-1}$ for the DTBT, DTBT:F, DTBT:Cl, DTBT:$CH_3$, DTBT:$OCH_3$, DTBT:OH, and DTBT:$NO_2$ molecular systems, respectively. These vibrational modes correspond to the C–C stretching of dithiophene. The excitation takes place from the low lying excited state ($S_1$) to the ground state ($S_0$) and gives the original vibrational state of the system under optical excitation [32].

### 3.4. FMOs analysis

The highest occupied molecular orbital energy (HOMO) defines the ability of electron giving, and the lowest unoccupied molecular orbital energy (LUMO) characterizes its ability of electron-accepting [33]. A molecule with a small HOMO–LUMO energy gap is usually related to low kinetic stability and high chemical reactivity and is also called a soft molecule [34]. To improve the performance of optoelectronic devices, $\pi$-conjugated materials with chemical modifications play a crucial role in fine-tuning the HOMO–LUMO energy gap. This, in turn, also fine-tunes the electro–optical properties of the molecular system [35].

In FMO diagram red color indicates a positive phase, and the green color indicates a negative phase. The FMOs of the DTBT, DTBT:F, DTBT:Cl, DTBT:$CH_3$, DTBT:$OCH_3$, DTBT:OH, and DTBT:$NO_2$ molecular systems are shown in Fig. 9. The FMOs of the DTBT molecule show the delocalization of electrons due to the overlapping orbitals of C–C and C=C atoms, leading to an increase in the HOMO level and a decrease in the LUMO level resulting in a low energy gap $\Delta E$ value of 2.74 eV (see Figs. 9 and 10).

The FMOs of DTBT calculated using CAM-B3LYP are shown in Fig. 10. The result of the FMO of DTBT is in good agreement with B3LYP and CAM-B3LYP. The HOMO value of $OCH_3$, OH, and $CH_3$ substituted molecules have a larger contribution to the D–A unit, and the LUMO value of F, Cl, OH, and $NO_2$ have a smaller contribution to the D–A unit. On the other hand, the electron density LUMO refers to almost all the substituents F, Cl, and the oxygen atom

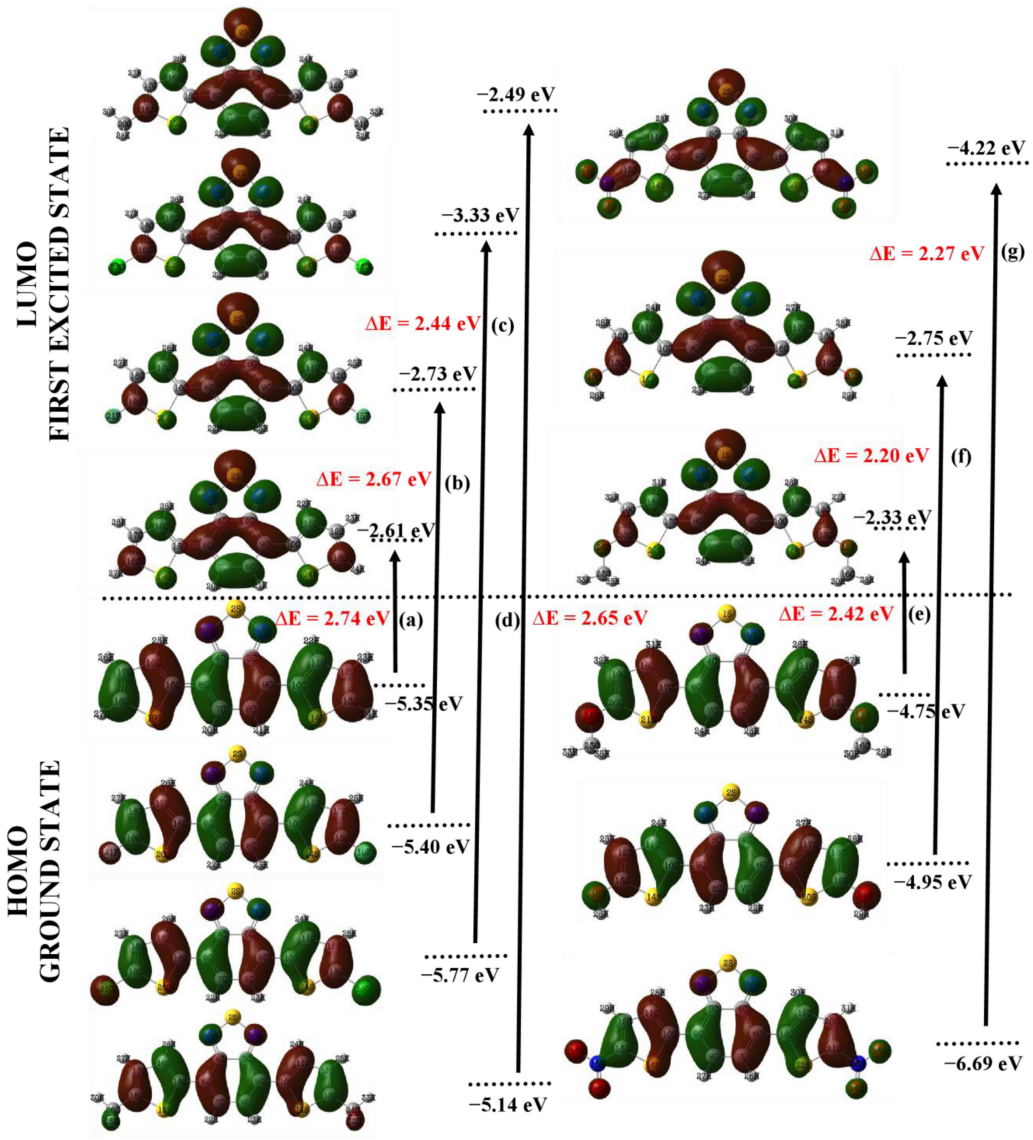


Fig. 9. The FMOs of (a) DTBT, (b) DTBT:F,(c) DTBT:Cl, (d) DTBT:$CH_3$, (e) DTBT:$OCH_3$,(f) DTBT:OH and (g) DTBT:$NO_2$ molecular systems, obtained using B3LYP/6-311+G$(d,p)$.

of $OCH_3$, OH, and $NO_2$ groups and their negligible contribution to $CH_3$, as a strong donating tendency of D–A unit to the substituents as acceptors is expected. In the case of substituted molecular systems, the energy gap values were calculated as 2.74, 2.67, 2.44, 2.65, 2.42, 2.20, and 2.27 eV for the molecular systems DTBT, DTBT:F, DTBT:$CH_3$, DTBT:Cl, DTBT:$OCH_3$, DTBT:$NO_2$, and DTBT:OH, respectively. The calculated smaller energy gap value of the investigated molecular systems is more favorable for the electronic transition, and also indicates the higher charge carrier mobility in the investigated systems as compared to the parent DTBT molecule [36]. The reduction in energy gap 2.27 eV along with enhancement of HOMO value 6.69 eV in the gas phase indicates that DTBT:$NO_2$ has higher first-order hyperpolarizability [26].

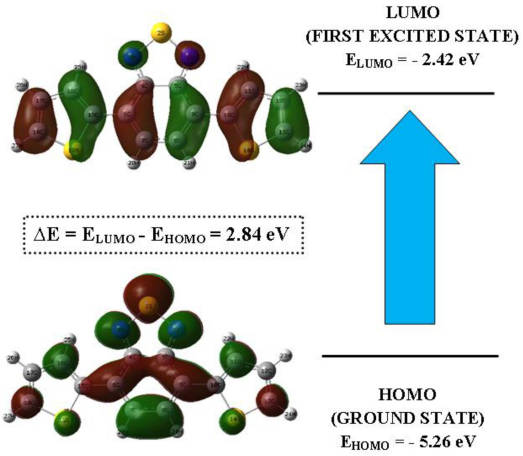


Fig. 10. The FMOs of DTBT molecular systems, obtained using CAM-B3LYP/6-311+G$(d,p)$.

TABLE X

The ionization potential, electron affinity and reorganization energy of electron and hole for the DTBT, DTBT:F, DTBT:Cl, DTBT:$CH_3$, DTBT:$OCH_3$, DTBT:OH, and DTBT:$NO_2$ molecular systems, calculated using B3LYP/6-311+G($d,p$) for singlet state ($E_S$). The symbol $E_g$ denotes energy gap; $IP_v$ — vertical ionization energy; $IP_a$ — adiabatic ionization energy; HEP-hole extraction potentials; $EA_v$ — vertical electron affinity; $EA_a$ — adiabatic electron affinity; and EEP — electron extraction potentials.

| Compound | HOMO [eV] | LUMO [eV] | $E_g$ [eV] | $IP_v$ [eV] | $IP_a$ [eV] | HEP [eV] | $EA_v$ [eV] | $EA_a$ [eV] | EEP [eV] | $\lambda_h$ [eV] | $\lambda_e$ [eV] |
|---|---|---|---|---|---|---|---|---|---|---|---|
| DTBT | 5.35 | 2.61 | 2.74 | 5.82 | 6.62 | 5.58 | 1.88 | 1.22 | 2.13 | 0.24 | 0.25 |
| DTBT:F | 5.40 | 2.73 | 2.67 | 5.91 | 6.56 | 5.73 | 1.92 | 1.35 | 2.15 | 0.17 | 0.23 |
| DTBT:Cl | 5.77 | 3.33 | 2.44 | 6.96 | 6.71 | 6.79 | 1.77 | 1.54 | 2.01 | 0.17 | 0.24 |
| DTBT:$CH_3$ | 5.14 | 2.49 | 2.65 | 5.59 | 6.34 | 5.33 | 1.73 | 1.15 | 2.00 | 0.26 | 0.27 |
| DTBT:$OCH_3$ | 4.75 | 2.33 | 2.42 | 5.31 | 5.88 | 5.09 | 1.31 | 1.01 | 1.54 | 0.22 | 0.23 |
| DTBT:OH | 4.95 | 2.75 | 2.20 | 6.09 | 6.32 | 5.99 | 1.29 | 1.17 | 1.43 | 0.09 | 0.14 |
| DTBT:$NO_2$ | 6.69 | 4.22 | 2.27 | 7.81 | 7.60 | 7.62 | 2.62 | 2.57 | 2.84 | 0.19 | 0.22 |

### 3.5. Ionization potential, electron affinity and re-organization energy

In general, the p-type organic semiconductors have lower ionization potential (IP) values, which allows the hole injection ability from the anode to the hole transport layer (HTL). Conversely, the n-type organic semiconductors have a higher electron affinity (EA) value, which allows the electron injection ability from the cathode to the electron transport layer (ETL). To check the hole and electron injection ability of the investigated systems, the HTL anode material indium tin oxide (ITO) with work function of 4.7 eV and the cathode bilayer material (Al/LiF) with work function of 3.1 eV are taken as in [37, 38]. In general, the energy difference between the work function of ITO 4.7 eV and the HOMO of HTML should be small for better hole injection. In the present case (Table X), the energy difference between work function of ITO 4.7 eV and HOMO of DTBT, DTBT:F, DTBT:Cl, DTBT:$CH_3$, DTBT:$OCH_3$, DTBT:OH, and DTBT:$NO_2$ molecular systems are calculated as 0.65, 0.7, 1.07, 0.44, 0.05, 0.25, and 1.99 eV, respectively.

The vertical ionization energy ($IP_v$) values of the investigated systems are calculated in the singlet state (see Table X) as in the order of DTBT:$OCH_3$ < DTBT:$CH_3$ < DTBT:F < DTBT:Cl < DTBT:OH < DTBT:$NO_2$, which also clearly indicates that the strongly interacting oxygen atom of DTBT:$OCH_3$ system can donate electrons to the D–A unit, resulting in an increase in the $\pi$-electron density in the D–A unit. Hence substitution of $OCH_3$ has a higher ability of electron injection to the D–A unit compared with all other investigated systems. The methoxy substitution on benzo[2,3-b]thiopene decreases the hole injection barrier to 6.84 eV and illuminating the methoxy group on 4,7-di-(2-thienyl)-2,1,3-benzothiadiazole further decreases it further, to 5.31 eV and less [15].

In addition, the calculated vertical electron affinity ($EA_v$) values of the investigated systems in the singlet state are given in Table X in the order of DTBT:$NO_2$ > DTBT:F > DTBT:Cl > DTBT:$CH_3$ > DTBT:$OCH_3$ > DTBT:OH. These values indicate that strongly influencing oxygen atom of $NO_2$ substitution on the DTBT molecule withdraws the electrons from the D–A unit, resulting in a decrease in the $\pi$-electron density in the D–A unit. Hence, substitution of $NO_2$ has the higher hole injection ability in the D–A unit compared with all other investigated systems. The nitro substitution on benzo[2,3-b]thiopene increases the electron injection barrier to 2.02 eV and illuminating the nitro group on 4,7-di-(2-thienyl)-2,1,3-benzothiadiazole increases it further, to 2.62 eV and more [15].

The increase in the adiabatic ionization energy ($IP_a$) values of the molecules in the triplet state for $NO_2$ > Cl > F shown in Table X, reveals the ability of these groups to have the withdrawing effect. The decrease in adiabatic electron affinity ($EA_a$) values of the molecules in the triplet state for OH < $OCH_3$ shown in Table XI, reveals the ability of these groups to have the donating effect. The results of DTBT and its substituents in a singlet state ($E_s$) are in good agreement with a triplet state ($E_t$), as listed in Tables X and XI. Most importantly, the triplet formation produces a higher driving voltage (0.25 to 0.27 eV) for the parent DTBT molecule compared to the singlet state (0.24 to 0.25 eV). It can be seen in Tables X and XI that the parent molecule DTBT and DTBT:$CH_3$ has the highest driving voltage compared to the other substituents in ($E_s$) and ($E_t$) states. It is correlated with Raman analysis and FMO evidencing intermolecular CT.

In general, the deformation geometry of the molecule and the transportability of charge carriers in organic molecules influence the reorganization energy. The reorganization energy of electron and hole

TABLE XI

The ionization potential, electron affinity and reorganization energy of electron and hole for the DTBT, DTBT:F, DTBT:Cl, DTBT:$CH_3$, DTBT:$OCH_3$, DTBT:OH, and DTBT:$NO_2$ molecular systems, calculated using B3LYP/6-311+G$(d,p)$ for triplet state ($E_T$). The symbol $E_g$ denotes energy gap; $IP_v$ — vertical ionization energy; $IP_a$ — adiabatic ionization energy; HEP-hole extraction potentials; $EA_v$ — vertical electron affinity; $EA_a$ — adiabatic electron affinity; and EEP — electron extraction potentials.

| Compound | HOMO [eV] | LUMO [eV] | $E_g$ [eV] | $IP_v$ [eV] | $IP_a$ [eV] | HEP [eV] | $EA_v$ [eV] | $EA_a$ [eV] | EEP [eV] | $\lambda_h$ [eV] | $\lambda_e$ [eV] |
|---|---|---|---|---|---|---|---|---|---|---|---|
| DTBT | 5.27 | 2.43 | 2.84 | 5.93 | 6.63 | 5.68 | 1.99 | 1.25 | 2.26 | 0.25 | 0.27 |
| DTBT:F | 5.39 | 2.65 | 2.74 | 5.81 | 6.74 | 5.63 | 1.95 | 1.38 | 2.16 | 0.18 | 0.21 |
| DTBT:Cl | 5.64 | 3.12 | 2.52 | 6.98 | 6.82 | 6.79 | 1.78 | 1.62 | 2.01 | 0.19 | 0.23 |
| DTBT:$CH_3$ | 5.18 | 2.52 | 2.66 | 5.55 | 6.45 | 5.29 | 1.76 | 1.15 | 2.01 | 0.26 | 0.25 |
| DTBT:$OCH_3$ | 4.87 | 2.30 | 2.57 | 5.62 | 5.81 | 5.40 | 1.39 | 1.05 | 1.10 | 0.22 | 0.29 |
| DTBT:OH | 4.98 | 2.65 | 2.33 | 6.05 | 6.22 | 5.98 | 1.22 | 1.14 | 1.34 | 0.07 | 0.12 |
| DTBT:$NO_2$ | 6.50 | 4.15 | 2.35 | 7.72 | 7.52 | 7.54 | 2.43 | 2.52 | 2.64 | 0.18 | 0.21 |

in the DTBT, DTBT:F, DTBT:Cl, DTBT:$CH_3$, DTBT:$OCH_3$, DTBT:OH, and DTBT:$NO_2$ molecular systems are computed by DFT/B3LYP method with 6-311+G$(d,p)$ basis set. The inter and intramolecular transfer of hole and electron can be represented as

$$\lambda_h = \lambda_+ + \lambda_0 = \Big[E^{ion}(Q_n) - E^0(Q_n)\Big] + \Big[E^{ion}(Q_c) - E^0(Q_c)\Big] = IP_v - HEP, \quad (1)$$

$$\lambda_e = \lambda_- - \lambda_0 = \Big[E^{ion}(Q_n) - E^0(Q_n)\Big] - \Big[E^{ion}(Q_c) - E^0(Q_c)\Big] = EEP - EA_v, \quad (2)$$

where $E^{ion}(Q_n)$ and $E^{ion}(Q_c)$ are the energy of the neutral and charged molecule in the cationic and anionic geometry, respectively. In the ground state, their respective energies are denoted as $E^0Q_n)$ and $E^0(Q_c)$.

According to the Marcus theory, it is noted that a higher charge transfer takes place when the $\lambda$ value becomes smaller. The computed $\lambda_h$ and $\lambda_e$ values of di-thienyl benzothiadiazole are equivalent to di-thienyl benzothiazole ($\lambda_h = 0.24$ eV and $\lambda_e = 0.25$ eV) [7]. The computed $\lambda_h$ and $\lambda_e$ values have shown that the hole reorganization energy is smaller than the electron reorganization energy. This confirms that the hole transport rate of the molecule has increased after the addition of substituents. The DTBT:F, DTBT:Cl, and DTBT:$NO_2$ molecular systems have higher hole transportability. Significantly, the DTBT:OH molecular system has both higher hole and electron transportability. Hence, these molecules can be used as potent hole transport materials compared to the substitution effect of F, Cl, $CH_3$, $OCH_3$, OH, and $NO_2$ at various positions on benzo[2,3-b]thiopene [15].

### 3.6. Natural bond orbital analysis

Natural bond orbital (NBO) analysis is a prominent method to identify conjugative interactions quantitatively. It also elucidates the donor–acceptor interactions between electron donor orbital and electron acceptor orbital from second-order micro disturbance theory. The occupied Lewis-type (bond or lone pair) and unoccupied non-Lewis-type (anti-bonding) natural bond orbitals undergo delocalization of $\pi$-electron density in the conjugated core of the molecule corresponding to stabilizing donor–acceptor interactions [39]. The stabilization energy was calculated as

$$E(2) = \Delta E_{ij} = q_i \frac{F(i,j)^2}{\varepsilon_i - \varepsilon_j}. \quad (3)$$

In the present case, the calculated stabilization energy E(2) values associated with the delocalization of each donor (i) to acceptor (j) of the DTBT, DTBT:F, DTBT:Cl, DTBT:$CH_3$, DTBT:$OCH_3$, DTBT:OH, and DTBT:$NO_2$ molecular systems were listed in Table XII. Higher stabilization energy values of the DTBT, DTBT:F, DTBT:Cl, DTBT:$CH_3$, DTBT:$OCH_3$, DTBT:OH, and DTBT:$NO_2$ molecular systems were calculated as 25.79, 21.77, 12.05, 5.91, 30.47, 28.03, and 174.84 Kcal/mol, respectively. These values correspond to the transitions of $\sigma$ (C6–C7) $\rightarrow$ $\sigma^*$ (N3–C4), LP (F15) $\rightarrow$ $\sigma^*$ (C12–C13), LP (Cl15) $\rightarrow$ $\sigma^*$ (C12–C13), $\pi$ (C20–H30) $\rightarrow$ $\pi^*$ (C18–S19), LP (O15) $\rightarrow$ $\sigma^*$ (C12–C13), LP (O15) $\rightarrow$ $\sigma^*$ (C12–C13), and LP (O17) $\rightarrow$ $\sigma^*$ (N15–O16). Calculated higher stabilizing energy values of the DTBT:$OCH_3$, DTBT:OH, and DTBT:$NO_2$ molecular systems indicate that these molecular systems can exhibit higher first-order polarizability values.

In the present NBO analysis, it is found that in DTBT:$OCH_3$ and DTBT:OH molecular systems, the lone pairs of the oxygen atom (O15), (O22) and (O15), (O21) interact with the antibonding

TABLE XII

The stabilization energy $E(2)$ values associated with the delocalization of each donor (i) to acceptor (j) of the DTBT, DTBT:F, DTBT:Cl, DTBT:$CH_3$, DTBT:$OCH_3$, DTBT:OH, and DTBT:$NO_2$ molecular systems, calculated using NBO analysis with B3LYP/6-311+G$(d,p)$. ED represent electron density.

| Molecule | Donor (i) | ED (i) | Acceptor (j) | ED (j) | $E(2)$ [Kcal/mol] | $E(\mathrm{j}) - E(\mathrm{i})$ [arb. units] |
|---|---|---|---|---|---|---|
| DTBT | $\sigma$ (N1–C5) | 1.8255 | $\sigma^*$ (N3–C4) | 0.4353 | 13.74 | 0.32 |
| | $\sigma$ (C6–C7) | 1.7122 | $\sigma^*$ (N3–C4) | 0.4353 | 25.79 | 0.24 |
| | $\sigma$ (C8–C9) | 1.7121 | $\sigma^*$ (C6–C7) | 0.3053 | 17.89 | 0.29 |
| | $\sigma$ (C12–C13) | 1.9868 | $\sigma^*$ (C10–C11) | 0.3348 | 15.81 | 0.30 |
| | LP (S2) | 1.5045 | $\sigma^*$ (N1–C5) | 0.4353 | 19.41 | 0.25 |
| | LP (S2) | 1.5045 | $\sigma^*$ (N3–C4) | 0.4353 | 19.41 | 0.25 |
| | LP (S14) | 1.9839 | $\sigma^*$ (C10–C11) | 0.3348 | 19.52 | 0.27 |
| | LP (S14) | 1.9839 | $\sigma^*$ (C12–C13) | 0.2923 | 21.65 | 0.27 |
| | LP (S19) | 1.9839 | $\sigma^*$ (C15–C16) | 0.3348 | 19.52 | 0.27 |
| | LP (S19) | 1.9839 | $\sigma^*$ (C17–C18) | 0.2923 | 21.64 | 0.27 |
| DTBT:F | LP (F15) | 1.9519 | $\pi^*$ (C12–C13) | 0.0272 | 5.92 | 1.01 |
| | LP (F15) | 1.9519 | $\pi^*$ (C13–S14) | 0.0473 | 11.67 | 0.63 |
| | LP (F15) | 1.9519 | $\sigma^*$ (C12–C13) | 0.3265 | 21.77 | 0.43 |
| | LP (F21) | 1.9519 | $\pi^*$ (C18–C19) | 0.0272 | 5.92 | 1.01 |
| | LP (F21) | 1.9519 | $\pi^*$ (C19–C20) | 0.0473 | 11.67 | 0.63 |
| | LP (F21) | 1.9519 | $\sigma$ (C17–C18) | 0.3265 | 21.77 | 0.43 |
| DTBT:Cl | LP (Cl15) | 1.9924 | $\pi^*$ (C12–C13) | 0.0242 | 2.74 | 0.91 |
| | LP (Cl15) | 1.9924 | $\pi^*$ (C13–S14) | 0.4560 | 7.29 | 0.46 |
| | LP (Cl15) | 1.9924 | $\sigma^*$ (C12–C13) | 0.3124 | 12.05 | 0.32 |
| | LP (Cl21) | 1.9924 | $\pi^*$ (C18–C19) | 0.0242 | 2.74 | 0.91 |
| | LP (Cl21) | 1.9924 | $\pi^*$ (C15–S20) | 0.4560 | 7.29 | 0.46 |
| | LP (Cl21) | 1.9924 | $\sigma^*$ (C18–C19) | 0.3124 | 12.05 | 0.32 |
| DTBT:$CH_3$ | $\pi$ (C20–H28) | 1.9808 | $\pi^*$ (C17–C18) | 0.0211 | 2.04 | 1.11 |
| | $\pi$ (C20–H29) | 1.9808 | $\pi^*$ (C17–C18) | 0.0211 | 2.04 | 1.11 |
| | $\pi$ (C20–H30) | 1.9834 | $\pi^*$ (C18–S19) | 0.0309 | 5.91 | 0.73 |
| | $\pi$ (C21–H31) | 1.9808 | $\pi^*$ (C12–C13) | 0.0211 | 2.04 | 1.11 |
| | $\pi$ (C21–H32) | 1.9808 | $\pi^*$ (C12–C13) | 0.0211 | 2.04 | 1.11 |
| | $\pi$ (C21–H33) | 1.9835 | $\pi^*$ (C13–S14) | 0.0309 | 5.91 | 0.73 |
| DTBT:$OCH_3$ | LP (O15) | 1.9472 | $\pi^*$ (C13–S14) | 0.0525 | 11.61 | 0.75 |
| | LP (O15) | 1.9472 | $\sigma^*$ (C12–C13) | 0.3523 | 30.47 | 0.34 |
| | LP (O15) | 1.9472 | $\pi^*$ (C16–H29) | 0.0186 | 5.14 | 0.74 |
| | LP (O22) | 1.9472 | $\pi^*$ (C20–S21) | 0.0525 | 11.61 | 0.75 |
| | LP (O22) | 1.9472 | $\sigma^*$ (C19–C20) | 0.3523 | 30.47 | 0.34 |
| | LP (O22) | 1.9472 | $\pi^*$ (C23–H25) | 0.0186 | 5.14 | 0.74 |
| DTBT:OH | LP (O15) | 1.9636 | $\pi^*$ (C13–S14) | 0.0505 | 9.92 | 0.76 |
| | LP (O15) | 1.9636 | $\sigma^*$ (C12–C13) | 0.3148 | 28.03 | 0.35 |
| | LP (O15) | 1.9636 | $\pi^*$ (C19–S20) | 0.0505 | 9.92 | 0.76 |
| | LP (O21) | 1.9636 | $\sigma^*$ (C18–C19) | 0.3148 | 28.03 | 0.35 |

TABLE XII cont.

| Molecule | Donor (i) | ED (i) | Acceptor (j) | ED (j) | $E(2)$ [Kcal/mol] | $E(j) - E(i)$ [arb. units] |
|---|---|---|---|---|---|---|
| DTBT:$NO_2$ | LP (O16) | 1.9998 | $\pi^*$ (C13–N15) | 0.0838 | 4.32 | 1.12 |
| | LP (O16) | 1.9998 | $\pi^*$ (C13–N15) | 0.0838 | 8.63 | 0.60 |
| | LP (O16) | 1.9998 | $\pi^*$ (N15–O17) | 0.0585 | 18.75 | 0.62 |
| | LP (O17) | 1.9998 | $\pi^*$ (C13–N15) | 0.0838 | 3.93 | 1.12 |
| | LP (O17) | 1.9998 | $\pi^*$ (C13–N15) | 0.0838 | 10.03 | 0.59 |
| | LP (O17) | 1.9998 | $\pi^*$ (N15–O16) | 0.0585 | 17.81 | 0.61 |
| | LP (O17) | 1.9998 | $\sigma^*$ (N15–O16) | 0.6969 | 174.84 | 0.11 |
| | LP (O24) | 1.9825 | $\pi^*$ (C21–N23) | 0.0838 | 4.38 | 1.12 |
| | LP (O24) | 1.9825 | $\pi^*$ (C21–N23) | 0.0838 | 8.63 | 0.60 |
| | LP (O24) | 1.9825 | $\pi^*$ (N23–O25) | 0.0585 | 18.75 | 0.62 |
| | LP (O25) | 1.9829 | $\pi^*$ (C21–N23) | 0.0838 | 3.93 | 1.12 |
| | LP (O25) | 1.9829 | $\pi^*$ (C21–N23) | 0.0838 | 10.03 | 0.59 |
| | LP (O25) | 1.9829 | $\pi^*$ (N23–O24) | 0.0589 | 17.81 | 0.61 |
| | LP (O25) | 1.9829 | $\sigma^*$ (N23–O24) | 0.6969 | 174.84 | 0.11 |

TABLE XIII

The stabilization energy $E(2)$ values associated with the delocalization of each donor (i) to acceptor (j) of the DTBT, DTBT:F, DTBT:Cl, DTBT:$CH_3$, DTBT:$OCH_3$, DTBT:OH, and DTBT:$NO_2$ molecular systems, calculated using NBO analysis with CAM-B3LYP/6-311+G$(d,p)$.

| Molecule | Donor (i) | ED (i) | Acceptor (j) | ED (j) | $E(2)$ [Kcal/mol] | $E(j) - E(i)$ [arb. units] |
|---|---|---|---|---|---|---|
| DTBT | $\sigma$ (N1–C5) | 1.8255 | $\sigma^*$ (N3–C4) | 0.4445 | 12.84 | 0.32 |
| | $\sigma$ (C6–C7) | 1.7122 | $\sigma^*$ (N3–C4) | 0.4256 | 23.62 | 0.24 |
| | $\sigma$ (C8–C9) | 1.7121 | $\sigma^*$ (C6–C7) | 0.3053 | 17.89 | 0.28 |
| | $\sigma$ (C12–C13) | 1.9868 | $\sigma^*$ (C10–C11) | 0.3328 | 15481 | 0.20 |
| | LP (S2) | 1.5045 | $\sigma^*$ (N1–C5) | 0.4363 | 17.41 | 0.25 |
| | LP (S2) | 1.5045 | $\sigma^*$ (N3–C4) | 0.4253 | 14.41 | 0.25 |
| | LP (S14) | 1.9839 | $\sigma^*$ (C10–C11) | 0.3448 | 19.52 | 0.21 |
| | LP (S14) | 1.9839 | $\sigma^*$ (N1–C5) | 0.2429 | 20.65 | 0.23 |
| | LP (S19) | 1.9839 | $\sigma^*$ (N3–C4) | 0.2348 | 19.52 | 0.27 |
| | LP (S19) | 1.9839 | $\sigma^*$ (C10–C11) | 0.2823 | 21.64 | 0.27 |

orbitals of the atoms in the D–A unit, establishing a strong inter- and intramolecular interactions with the increase in hyperpolarizability. In the molecular system, DTBT:$NO_2$ molecular, the lone pair of nitrogen atoms (N15) and (N23) interacts with disubstituted antibonding orbitals of the oxygen atom (O16) and (O24) to establish strong intramolecular interactions, which lead to a high degree of first-order hyperpolarizability. Hence, these molecular systems can be useful for designing novel NLO materials. The result of DTBT is in good agreement with B3LYP/CAM-B3LYP listed in Table XIII.

### 3.7. Natural population analysis

The charge transfer between the D–A unit and substituted groups of the DTBT molecule was studied using atomic charges, which were calculated using the natural population analysis (NPA). The NPA charge values of the DTBT molecule calculated using B3LYP are listed in Table XIV and are in good agreement with those obtained with CAM-B3LYP, listed in Table XV. The calculated NPA charge values of the carbon atoms vary from −0.0868 to 0.1951, those of the hydrogen atoms — from 0.2419 to 0.5033, and those of the

TABLE XIV

NPA charge values of the DTBT molecule, calculated using B3LYP/6-311+G$(d,p)$.

| Atoms | NPA charges | Atoms | NPA charges | Atoms | NPA charges |
|---|---|---|---|---|---|
| N1 | −0.5599 | C10 | −0.1807 | S19 | 0.2815 |
| S2 | 0.7133 | C11 | −0.2197 | H20 | 0.2419 |
| N3 | −0.5599 | C12 | −0.3552 | H21 | 0.2419 |
| C4 | 0.1738 | C13 | 0.1951 | H22 | 0.2758 |
| C5 | 0.1738 | S14 | 0.2815 | H23 | 0.2577 |
| C6 | −0.0869 | C15 | −0.1806 | H24 | 0.5033 |
| C7 | −0.2060 | C16 | −0.2197 | H25 | 0.2757 |
| C8 | −0.2060 | C17 | −0.3552 | H26 | 0.2577 |
| C9 | −0.0868 | C18 | 0.1951 | H27 | 0.5033 |

TABLE XV

NPA charge values of the DTBT molecule, calculated using CAM-B3LYP/6-311+G$(d,p)$.

| Atoms | NPA charges | Atoms | NPA charges | Atoms | NPA charges |
|---|---|---|---|---|---|
| N1 | −0.5569 | C10 | −0.1827 | S19 | 0.2615 |
| S2 | 0.6133 | C11 | −0.2127 | H20 | 0.2349 |
| N3 | −0.5599 | C12 | −0.3554 | H21 | 0.2419 |
| C4 | 0.1738 | C13 | 0.1951 | H22 | 0.2758 |
| C5 | 0.1721 | S14 | 0.2816 | H23 | 0.2577 |
| C6 | −0.0869 | C15 | −0.1807 | H24 | 0.4033 |
| C7 | −0.1060 | C16 | −0.2197 | H25 | 0.2757 |
| C8 | −0.2060 | C17 | −0.3552 | H26 | 0.2578 |
| C9 | −0.0868 | C18 | 0.1951 | H27 | 0.5034 |

sulphur atoms — from 0.2815 to 0.7133. Significantly, a higher positive charge value of the DTBT molecule is predicted for the atom S2 (0.7133), and a higher negative charge value of the molecule was obtained for the atoms N1 and N3 (−0.5599). The sulphur atoms of the DTBT molecule lose electrons, which makes atoms N1 and N3 more electronegative. In addition, the carbon atoms have both positive and negative charge values, and notably, the electronegativity of the carbon atoms has fewer values compared to that of nitrogen atoms of the DTBT molecule.

Moreover, the calculated NPA charges of the D–A ring and substituent group in the DTBT:F, DTBT:Cl, DTBT:$CH_3$, DTBT:$OCH_3$, DTBT:OH, and DTBT:$NO_2$ molecular systems were listed in Table XVI. It is interesting to note that next to DTBT:$NO_2$, the highest NPA charge value was predicted for the DTBT:F and DTBT:Cl molecules, which is due to the charge transfer from the D–A unit to the substituted groups. Moreover, doping of halogen atoms enhances the electron charge carrier mobility from the D–A unit to the substituted groups, which also presents that the substituted F and Cl groups can withdraw the electrons easily from the D–A unit [40].

## 4. NLO analysis

In the case of $\pi$-conjugated molecules, they exhibit an asymmetric polarization effect that creates an induced dipole moment by mixing electron donor and electron acceptor groups. Therefore $\pi$-conjugated molecules are potential candidates for NLO applications. The electric dipole moment ($\boldsymbol{\mu}$) and first-order hyperpolarizability ($\beta$) values were calculated based on the finite field approach. The first-order hyperpolarizability is a third-rank tensor, which can be described by a 3D matrix and can be reduced to 10 components due to the Kleinman symmetry in a lower tetrahedral format [41].

The total static dipole moment ($\mu_{\text{tot}}$) and the mean first-order hyperpolarizability $\beta$ using the $x$, $y$, and $z$ components are defined accordingly:

- dipole moment

$$\mu_{\text{tot}} = \left(\mu_x^2 + \mu_y^2 + \mu_z^2\right)^{1/2}, \tag{4}$$

- first-order hyperpolarizability

$$\beta = \left(\beta_x^2 + \beta_y^2 + \beta_z^2\right)^{1/2}, \tag{5}$$

where

$$\beta_x = (\beta_{xxx} + \beta_{xyy} + \beta_{xzz}),$$

$$\beta_y = (\beta_{yyy} + \beta_{yzz} + \beta_{yxx}),$$

$$\beta_z = (\beta_{zzz} + \beta_{zxx} + \beta_{zyy}). \tag{6}$$

Thus,

$$\beta = \Big[\left(\beta_{xxx} + \beta_{xyy} + \beta_{xzz}\right)^2 + \left(\beta_{yyy} + \beta_{yzz} + \beta_{yxx}\right)^2 + \left(\beta_{zzz} + \beta_{zxx} + \beta_{zyy}\right)^2\Big]^{1/2}. \tag{7}$$

The calculated values of $\mu$ and $\beta$ for the DTBT, DTBT:F, DTBT:Cl, DTBT:$CH_3$, DTBT:$OCH_3$, DTBT:OH, and DTBT:$NO_2$ molecular systems are listed in Table XVII. The dipole moment and first-order hyperpolarizability values of urea, respectively, 1.3793 D and $3.734 \times 10^{-31}$ esu, were calculated using the B3LYP method with 6-311G$(d,p)$ basis set [42]. The dipole moment values of

TABLE XVI

NPA charge values of the D–A ring and substituent group in the DTBT:F, DTBT:Cl, DTBT:$CH_3$, DTBT:$OCH_3$,DTBT:OH, and DTBT:NO molecular systems, calculated using B3LYP/6-311+G$(d,p)$.

| Molecules | D–A ring[a,b] | Substituent group[b] |
|---|---|---|
| DTBT:F | 0.097 | −0.288 |
| DTBT:Cl | 0.081 | −0.286 |
| DTBT:$CH_3$ | −0.194 | 0.013 |
| DTBT:$OCH_3$ | −0.148 | −0.098 |
| DTBT:OH | ±0.198 | ±0.252 |
| DTBT:$NO_2$ | 0.098 | −0.291 |

[a]overall charges of D–A unit, [b]electric charges expressed in terms of elementary charge (e).

TABLE XVII

The dipole moment ($\boldsymbol{\mu}$) and first-order hyperpolarizability ($\beta$) values of the DTBT, DTBT:F, DTBT:Cl, DTBT:$CH_3$, DTBT:$OCH_3$, DTBT:OH, and DTBT:$NO_2$ molecular systems, calculated using B3LYP/6-311+G$(d,p)$.

| NLO parameters | DTBT | DTBT:F | DTBT:Cl | DTBT:$CH_3$ | DTBT:$OCH_3$ | DTBT:OH | DTBT:$NO_2$ |
|---|---|---|---|---|---|---|---|
| $\mu_x$ | 0.001 | −0.001 | −0.001 | 0.000 | 0.000 | −0.001 | −0.000 |
| $\mu_y$ | −0.135 | 1.105 | 1.515 | −0.641 | −3.561 | −2.947 | 5.165 |
| $\mu_z$ | 0.006 | 0.001 | 0.001 | 0.000 | 0.001 | 0.000 | −0.001 |
| $\mu_{\text{tot}}$ | 0.135 | 1.105 | 1.515 | 0.641 | 3.561 | 2.947 | 5.165 |
| $\beta_{xxx}$ | −0.008 | −0.003 | −0.000 | 0.000 | −0.000 | −0.012 | −0.008 |
| $\beta_{xxy}$ | −15.157 | 59.619 | 71.194 | −35.287 | −155.981 | −115.367 | 252.934 |
| $\beta_{xyy}$ | 0.003 | −0.000 | −0.001 | 0.000 | 0.000 | −0.007 | −0.001 |
| $\beta_{yyy}$ | 16.199 | −2.043 | 14.272 | 16.115 | −34.449 | −40.452 | 49.109 |
| $\beta_{xxz}$ | 0.041 | 0.018 | 0.012 | 0.006 | 0.069 | −0.014 | −0.036 |
| $\beta_{xyz}$ | −3.103 | 0.001 | −0.011 | −0.002 | −0.044 | −0.053 | −0.012 |
| $\beta_{yyz}$ | 0.002 | −0.001 | 0.003 | 0.002 | 0.009 | −0.029 | −0.002 |
| $\beta_{xzz}$ | 0.001 | 0.000 | −0.002 | 0.000 | 0.000 | −0.001 | −0.000 |
| $\beta_{yzz}$ | 7.429 | −3.999 | −0.687 | 3.325 | −3.129 | −0.089 | −9.787 |
| $\beta_{zzz}$ | −0.049 | −0.006 | −0.000 | 0.001 | 0.007 | −0.007 | 0.001 |
| $\beta_{\text{tot}}$ ($\times 10^{-31}$) | 0.731 | 0.146 | 7.324 | 1.369 | 137.672 | 13.469 | 292.256 |

TABLE XVIII

The dipole moment ($\boldsymbol{\mu}$) and first-order hyperpolarizability ($\beta$) values of the DTBT molecular systems, calculated using CAM-B3LYP/6-311+G$(d,p)$.

| NLO parameters | DTBT | NLO parameters | DTBT |
|---|---|---|---|
| $\mu_x$ | 0.021 | $\beta_{xxx}$ | −0.007 |
| $\mu_y$ | −0.125 | $\beta_{xxy}$ | −15.157 |
| $\mu_z$ | 0.002 | $\beta_{xyy}$ | 0.103 |
| $\mu_{\text{tot}}$ | 0.127 | $\beta_{yyy}$ | 16.198 |
| | | $\beta_{xxz}$ | 0.041 |
| | | $\beta_{xyz}$ | −3.113 |
| | | $\beta_{yyz}$ | 0.012 |
| | | $\beta_{xzz}$ | 0.011 |
| | | $\beta_{yzz}$ | 6.327 |
| | | $\beta_{zzz}$ | −0.049 |
| | | $\beta_{\text{tot}}$ ($\times 10^{-31}$) | 0.639 |

the DTBT:$OCH_3$, DTBT:OH, and DTBT:$NO_2$ molecular systems are calculated as 3.561, 2.947, and 5.165 D, which are 2.581, 2.136, and 3.744 times greater than urea, respectively. In addition, first-order hyperpolarizability values of the DTBT:$OCH_3$, DTBT:OH, and DTBT:$NO_2$ molecular systems were calculated as $137.672 \times 10^{-31}$, $13.469 \times 10^{-31}$, and $292.256 \times 10^{-31}$ esu, which are 36.870, 3.6.07, and 78.268 times greater than urea, respectively. Higher $mu$ and $\beta$ values were predicted for the DTBT:$NO_2$ molecule compared to that of all other investigated systems. Hence, the DTBT substituted molecules can be useful for future studies of NLO properties. The result of DTBT is in good agreement with those obtained with B3LYP/CAM-B3LYP listed in Table XVIII.

## 5. Conclusion

The molecular geometry and charge transfer analysis were investigated for the molecular systems DTBT, DTBT:F, DTBT:Cl, DTBT:$CH_3$, DTBT:$OCH_3$, DTBT:OH, and DTBT:$NO_2$. The vibrational properties of the investigated molecular systems, predicted using Raman spectral analysis, prove red shift pointing out the charge transfer upon substitutions.

The UV-Visible absorption and emission spectra of the investigated molecular systems validate the charge transfer from the D–A unit to the substituted groups. The frontier molecular orbital analysis confirms that the energy gap value of substituted molecules decreases after the addition of substituents, which eases the intramolecular charge transfer from the D–A unit to the substituted groups except for DTBT:$CH_3$. The ionization potential, electron affinity, and re-organization energy analyses indicate that the DTBT:OH molecular system has both higher hole and electron transportability compared with the parent DTBT molecule and other substituents. The natural bond orbital analysis proves higher stabilization energy for DTBT:$OCH_3$, DTBT:OH, and DTBT:$NO_2$ indicating that these molecular systems exhibit first-order hyperpolarizability. Hence these materials can be useful in designing potent NLO materials. The present study will be useful in the design of novel hole transport and NLO materials.

## References


[1] S. Telitel, F. Ouhib, J. Pierre Fouassier, *Macromol. Chem. Phys.* **215**, 1514 (2014).

[2] J. Cameron, L. Nanson, N. Blouin, N.J. Findlay, *Org. Electron.* **49**, 400 (2019).

[3] Y. Ait Aicha, S. Mohamed Bouzzine, Z.M Fahim, T. Zair, M. Bouachrine, M. Hamidi, *Comput. Theor. Chem* **1036**, 22 (2014).

[4] S. Dufresne, G.S. Hanan, W.G. Skene, *J. Phys. Chem. B* **111**, 11407 (2007).

[5] P. Ledwon, R. Motyka, K. Ivaniuk, A. Pidluzhna, N. Martyniuk, P. Stakhira, G. Baryshnikov, B.F. Minaev, H. Agren, *Dyes Pigm.* **173**, 108008 (2020).

[6] D. Sajan, K. Chaitanya, K. Safakath, R. Philip, T. Suthan, N.P. Rajesh, *Spectrachim. Acta A* **106**, 253 (2013).

[7] T. Sutradhar, A. Misra, *RSC Adv.* **10**, 40300 (2020).

[8] Y. Li, L. Yi Zou, A. MinRen, J. Kang Feng, *Comput. Theor. Chem.* **981**, 14 (2012).

[9] J.G. Mei, N.C. Heston, S.V. Vasilyeva, J.R. Reynols, *Macromolecules* **42**, 1482 (2009).

[10] J. Hung, Q. Liu, J.H. Zou, X.H. Zhu, *Adv. Funct. Mater* **19**, 1 (2009).

[11] I.B. Ceballos, F. Hermerschmidt, A.V. Alexander, D.K. Susarova, P.A. Troshin, S.A. Choulis, *Chem. Sus. Chem* **8** 4209 (2015).

[12] J. Ohshita, M. Miyazaki, D. Tanaka, Y. Morihara, Y. Fujitac, Y. Kunugi, *Polym. Chem.* **4**, 3116 (2013).

[13] E. Bundgaard, F.C. Krebs, *Macromolecules* **39**, 2823 (2006).

[14] Y. Pan, J. Huang, *RSC Adv.* **7**, 19576 (2017).

[15] A. Irfan, A.G. Al-Sehemi, M.S. Al-Assiri, *Comput. Theor. Chem.* **1031**, 76 (2014).

[16] E. Frisch, M.J. Frisch, F.R. Clemente et al., Gaussian 09 (now Gaussian 16), Gaussian Inc., Wallingford (CT) 2016.

[17] R. Dennigton, T. Keith, J. Millam, Gauss View 5.0 Semichem Inc., Shawnee Mission (KS) 2009.

[18] M.H. Jamroz, Vibrational Energy Distribution Analysis VEDA 4, Warsaw 2004.

[19] J. Demaison, A.G. Csaszar, *J. Mol. Struct.* **1023**, 7 (2012).

[20] E. J.J Martin, N. Berube, *J. Mater. Chem. C* **3**, 6058 (2015).

[21] P. Gumus, O. Tamer, D. Avci, Y. Atalay, *Indian J. Phys.* **90**, 79 (2016).

[22] E. Luzina, J. Sepioł, Y.N. Svartsov, A. Grabowska, *J. Chem. Phys.* **126**, 194308 (2007).

[23] M.F. Rode, A.L. Sobolewski, *J. Phys. Chem. A*, **114**, 11879 (2010).

[24] M.F. Rode, A.L. Sobolewski, *J. Chem. Phys.* **140**, 084301 (2014).

[25] S. Abdel Halim, A.K. Khalil, *J. Mol. Struct.* **114**, 651 (2017).

[26] S. Vijayalakshmi, S. Kalyanaraman, *Optik* **125**, 2429 (2014).

[27] D. Sajan, I. Hubert Joe, V.S. Jayakumar, *J. Raman Spectrosc.* **37**, 508 (2006).

[28] V. Hernández, J. Casado, *J. Chem. Phys.* **112**, 5105 (2000).

[29] P. Jha, S.P Koiry, V. Saxena, P. Veerender, A. Gusain, A.K. Chauhan, A.K. Debnath, D.K. Aswal, S.K. Gupta, *Org. Electron.* **14**, 2635 (2013).

[30] R.M. Silverstein, F.X. Webster, *Spectrometric Identification of Organic Compounds*, 6th ed., John Wiley & Son, 1998.

[31] V. Hernandez, S.C. Losada, J. Casdo, H. Higuchi, *J. Phys. Chem. A* **104**, 661 (2000).

[32] S. Wood, J.R. Hollis, Ji-Seon Kim, *J. Phys. D. Appl. Phys.* **50**, 073001 (2017).

[33] R. Premkumar, S. Hussain, T. Mathavan, K. Anitha, A. Milton Franklin Benial, *J. Mol. Liq.* **290**, 111209 (2019).

[34] V. Narayan, H.N. Mishra, O. Prasad, L. Sinha, *Comput. Theor. Chem.* **973**, 20 (2011).

[35] C. Coluccini, P.T Anusha, H. Yi Tiffany Chen, S. LunLiao, Y. Kuan Ko, A. Yabushita, C.W. Luo, Y.M. Ng, Y.L. Khung, *Sci. Rep.* **9**, 12762 (2019).

[36] P.L. Crossley, I.A. Cade, E.R. Clark, A. Escande, M.J. Humphries, S.M. King, I. Victorica-Yrezabal, M.J. Ingleson, M.L. Turner, *Chem. Sci* **6**, 5144 (2015).

[37] Y. Park, V. Choong, Y. Gao V. Choong, Y. Gao, *Appl. Phys. Lett.* **68**, 2699 (1996).

[38] Z. Sun, B. Ding, B. Wu, Y. You, X. Ding, X. Hou, *J. Phys. Chem. C* **3**, 2543 (2012).

[39] N.R. Sheela, S. Muthu, S. Sampathkrishnan, *Spectrochim. Acta A* **120**, 237 (2014).

[40] C. Ma, H. Li, Y. Yang, D. Li, Y. Liu, *Chem. Phys. Lett.* **638**, 72 (2015).

[41] D.A. Kleinman, *Phys. Rev.* **126**, 1977 (1962).

[42] M. Kurtz, M. Karabacak, S. Okur, S. Sayin, M. Yilmaz, N. Sundaraganesan, *Spectrochim. Acta A* **94**, 126 (2012).